JGR Planets

RESEARCH ARTICLE
10.1029/2018JE005701

Special Section:
5th International Planetary Dunes Workshop Special Issue

# Numerical Study of Shear Stress Distribution Over Sand Ripples Under Terrestrial and Martian Conditions

**A. Siminovich[1], T. Elperin[1], I. Katra[2], J. F. Kok[3], R. Sullivan[4], S. Silvestro[5,6], and H. Yizhaq[7]**

[1]Department of Mechanical Engineering, The Pearlstone Center for Aeronautical Engineering Studies, Ben-Gurion University of the Negev, Beersheba, Israel, [2]Department of Geography and Environmental Development, Ben-Gurion University of the Negev, Beersheba, Israel, [3]Department of Atmospheric and Oceanic Sciences, University of California, Los Angeles, CA, USA, [4]Cornell Center for Astrophysics and Planetary Sciences, Cornell University, Ithaca, NY, USA, [5]INAF Osservatorio Astronomico di Capodimonte, Napoli, Italy, [6]SETI Institute, Carl Sagan Center, Mountain View, CA, USA, [7]Swiss Institutes for Dryland Environmental and Energy Research, BIDR, Ben-Gurion University of the Negev, Midreshet Ben-Gurion, Beersheba, Israel

**Key Points:**
- Computational fluid dynamics experiments to model boundary layer shear stresses were applied to aeolian ripples under Earth and Mars conditions
- Shear velocities along Martian ripples did not reach fluid threshold, while at the crests of smaller terrestrial ripples, it was exceeded
- Fluid shear stress is a more important factor for controlling ripples size on Earth than on Mars

**Supporting Information:**
- Supporting Information S1

**Correspondence to:**
H. Yizhaq,
yiyeh@bgu.ac.il

**Citation:**
Siminovich, A., Elperin, T., Katra, I., Kok, J. F., Sullivan, R., Silvestro, S., & Yizhaq, H. (2019). Numerical study of shear stress distribution over sand ripples under terrestrial and Martian conditions. *Journal of Geophysical Research: Planets*, *124*, 175–185. https://doi.org/10.1029/2018JE005701

Received 24 MAY 2018
Accepted 5 JAN 2019
Accepted article online 15 JAN 2019
Published online 28 JAN 2019

**Author Contributions:**
**Conceptualization:** T. Elperin
**Formal analysis:** J. F. Kok
**Methodology:** T. Elperin, I. Katra, R. Sullivan
**Validation:** A. Siminovich
**Writing - original draft:** I. Katra, J. F. Kok, R. Sullivan, S. Silvestro

©2019. American Geophysical Union. All Rights Reserved.

**Abstract** Ripples occur on Earth and Mars in a range of sizes. From terrestrial studies, ripple size is known to depend on grain-size frequency, wind duration, wind strength (including stronger winds that can flatten ripples), and fundamental environmental factors that differ between the two planets. Here we use computational fluid dynamics (CFD) experiments to model boundary layer shear stresses applied to aeolian ripple surfaces, to investigate how these stresses might differ between Earth and Mars. CFD experiments used ANSYS Fluent, with inlet wind speeds of 10 and 15 m/s for both planetary environments. Ripple profiles for Earth and Mars were developed using saltation and reptation properties modeled by the numerical saltation model COMSALT (Kok & Renno, 2009, https://doi.org.10.1029/2009JDO11702) to develop ripple profiles using the numerical technique of Yizhaq et al. (2004, https://doi.org.10.1016/j.physd.2004.03.015). Although the CFD experiments using these inputs could not include the effects of a saltation cloud, results are robust enough to indicate clearly that for similar modeled wind speeds on Earth and Mars, boundary layer shear stress applied to ripple surfaces is greater on Earth under conditions for which sand transport is expected. These results indicate that ripples can grow larger on Mars than on Earth, because for typical Martian wind speeds the shear velocity at the ripple crests is below the fluid threshold.

**Plain Language Summary** Elucidating the origin of many natural patterns on Earth and planetary surfaces is a challenging problem of pattern formation in complex systems. Among these mysterious phenomena are the aeolian sand ripples, which are a common pattern of granular matter on Earth and on Mars. Ripple wavelength on Earth is <30 cm, and height is less than 1 cm, whereas on Mars they might be much larger both in wavelength and height. On Mars, two sizes of aeolian ripples were observed, small (decimeter scale) impact ripples like those on Earth and large, meter-scale ripples with no terrestrial analog. The large ripples on Mars were detected in orbital images and first visited in situ by the NASA Mars Exploration Rover Spirit at the El Dorado ripple field in Gusev Crater. The existence of very large ripples on Mars lacking exact terrestrial analogues is not fully understood at this time and is still a matter of conjecture and debate. In this study, computational fluid dynamics simulations over simulated sand ripples illustrate the differences in shear stress expected at ripple crests on Earth and Mars under two test flow wind speeds. The distribution of the shear stress over ripple crest is important for predicting the entrainment from the crest, which is one of several possible mechanisms for limiting ripple growth by removing grains from the crest, yet its relative importance on Earth and Mars is not understood. The Martian ripple profile was three times larger in the experiments than the terrestrial ripple profile but still several factors smaller than the largest ripples encountered by Mars rovers. Despite this, shear velocities along Martian ripple crests did not reach the critical velocity where erosion from the crest occurs, while at the crests of the smaller terrestrial ripples, the critical velocity was exceeded at the same test inlet wind speeds. These results indicate that fluid shear stress is a more important factor for controlling ripple size on Earth than on Mars and may help to explain why impact ripples on Mars can grow larger than on Earth. These results are useful for understanding the aeolian processes involved in ripple formation under Martian atmospheric conditions.

Further studies are needed to verify this conclusion for more realistic larger Martian ripples and for higher shear velocities.

## 1. Introduction

Aeolian impact or normal ripples are abundant on Earth and Mars. They develop from instability of a flatbed to the shear stress of wind on loose sand (Figure 1). Ripples develop in fine sand with a unimodal distribution, unlike megaripples, which require a bimodal distribution including significantly coarser material (Lämmel et al., 2018; Yizhaq et al., 2012). Ripple wavelength on Earth is <30 cm, and height is less than 1 cm, whereas on Mars they might be much larger both in wavelength and height (Bridges et al., 2012; Ewing et al., 2017; Lapotre et al., 2016, 2018a, 2018b; Silvestro et al., 2010, 2016; Sullivan et al., 2008). On Mars, two sizes of aeolian ripples have been observed, small (decimeter-scale) impact ripples like those on Earth (Sullivan et al., 2005; Yizhaq et al., 2014) and large, meter-scale ripples with no corresponding terrestrial analog (Bridges et al., 2012; Ewing et al., 2017; Lapotre et al., 2016). The large ripples on Mars have been detected in orbital images (Bridges et al., 2007; Malin & Edgett, 2001) and first visited in situ by the NASA Mars Exploration Rover Spirit at the El Dorado ripple field in Gusev Crater (Sullivan et al., 2008). Based on recent data sent by the NASA Mars Science Laboratory Curiosity rover in Gale Crater, Lapotre et al. (2016) gave an alternative hypothesis for the origin of the large (2.1 m in wavelength) ripples that superimpose the dune slopes. According to their theory, the large ripples visited by Curiosity are fluid drag ripples (Bagnold, 1941, pp. 165–166; Wilson, 1972) that form due to the large kinematic viscosity on Mars (Lapotre et al., 2016). In this scenario, the large Martian ripples are not just larger versions of terrestrial impact ripples, but rather analogues to current ripples (Allen, 1968) that form in unidirectional water streams on Earth (Lapotre et al., 2016). These large ripples cannot be megaripples because there is no discernable grain-size variation between the crest and slopes of the ripple (Ewing et al., 2017; Lapotre et al., 2016); thus, they would form a unique aeolian bedform according to this theory. However, based on numerical simulations for wind velocity near the threshold, Durán et al. (2014) predicted using a scaling law (equation (4) in their paper) that the impact ripple wavelength on Mars can be 20 times larger than impact ripples on Earth. Assuming a typical wavelength of terrestrial ripples to be 0.15 m means that ripples on Mars can grow up to 3-m wavelength without the need to explain their larger scale with the fluid drag theory.

Ripples form when the wind speed exceeds a certain threshold (known as the fluid threshold) and sand grains start to move, mostly through saltation and reptation (Anderson, 1987, 1990; Anderson & Bunas, 1993; Kok et al., 2012). However, due to the presence of saltators near the bed (the saltation layer), the shear velocity is reduced below the fluid threshold, and steady state saltation is maintained due to the impact mechanism (Kok et al., 2012). In steady state saltation, saltators move in a cascade of asymmetric ballistic trajectories and are accelerated by the wind and, when reimpacting and rebounding from the bed, eject low-energy grains that hop just once. When the latter grains return to the surface, they neither rebound nor disturb others, but they can roll short distances on the order of a few millimeters. This mode of sand transport is known as reptation (Anderson, 1987, 1990; Durán et al., 2014).

Ripple dimensions (height and wavelength) develop over time until reaching a steady state size at which ripples migrate downwind with a velocity (celerity) that increases linearly with wind speed (Andreotti et al., 2006; Rasmussen et al., 2015). In this steady state the deposition of grains at the crest is balanced by erosion due to the speedup of wind velocity at the crest (Bagnold, 1941, pp. 151–153; Bar et al., 2016). The final size of ripples thus depends on the shear velocity on the crest, on the grain diameter, and on the impact angle of saltating particles (Anderson, 1987; Andreotti et al., 2006; Bagnold, 1941; Durán et al., 2014; Schmerler et al., 2016; Seppälä & Lindé, 1978; Sharp, 1963). Ripples will be flattened when the shear velocity at the surface exceeds the fluid threshold (Bar et al., 2016).

Due to the low density atmosphere on the surface of Mars the fluid shear velocity, $u_{*t}$, needed for direct entertainment of grains into saltation is much higher than on Earth as shown in Figure 2 (Greeley et al., 1980; Iversen & White, 1982; cf. Shao & Lu, 2000; Kok, 2010a; Kok, 2010b; Kok et al., 2012). The shear velocity, $u_*$, a measure of the wind stress defined as $u_* = \sqrt{\tau/\rho_a}$where $\rho_a$ is the air/atmosphere density and $\tau$ is

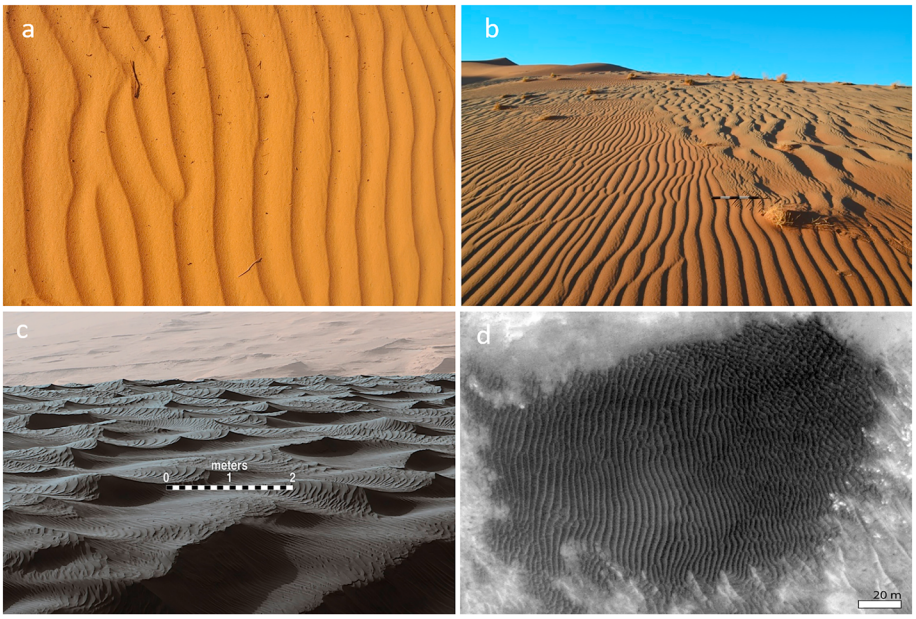


**Figure 1.** Aeolian ripples on Earth and Mars. (a) Impact ripples at Nizzana sand dunes at the western Negev near the border between Israel and Egypt (the average wavelength is about 10 cm). (b) A sharp transition between almost straight normal ripples (left) and wavy megaripples (right) on the downwind slope of a dune at Sossusvlei, Namibia (the scale bar is 0.5 m long). (c) Two sizes of ripples are evident in this 13 December 2015, view of the top of a Martian sand dune, from the Curiosity rover at Gale crater. (d) Very large ripples of the El Dorado ripple aeolian deposit at Gusev crater, visited by Mars Exploration Rover Spirit rover.

the shear stress. However, on Mars there is a large discrepancy between the fluid threshold and the impact threshold, $u_{*ti}$, which is the shear velocity needed to sustain saltation by the impact mechanism (Claudin & Andreotti, 2006; Kok, 2010b: Yizhaq et al., 2014). On Earth the ratio is $u_{*ti}/u_{*t} \simeq 0.8$ while on Mars it is much smaller, $u_{*ti}/u_{*t} \simeq 0.1$ (Kok et al., 2012). It has been suggested that this difference can explain the large aeolian activity observed on Mars despite the low predicted wind velocities (Kok, 2010b; Kok et al., 2012; Silvestro et al., 2011; Sullivan & Kok, 2017). Global climate models for Mars, because of their low spatial resolution, generally do not predict $u_* > u_{*t}$, and thus, no sand transport should occur (Basu et al., 2004; Chojnacki et al., 2011). Even the MarsWRF model with a spatial resolution of ~ 490 m cannot resolve small-scale turbulent effects and subgrid topography, hence can underestimate surface wind strength (Baker et al., 2018). The few and infrequent wind measurements made by Mars landers have also found that winds on Mars rarely exceed the fluid threshold needed for initiation of sand transport (Holstein-Rathlou et al., 2010; Schofield et al., 1997; Zimbelman, 2000). Recently, a mechanism was identified for low-flux sand transport on Mars occurring close to $u_{*ti}$ without the need for gusts above the fluid threshold to initiate the saltation (Sullivan & Kok, 2017). This mechanism is based on sporadic saltation clusters formed above the impact threshold but well below the fluid threshold, over long fetch lengths where the grains hop on the surface with increasing energy due to the low Martian gravity. These clusters can affect a narrow zone of surface grains and should result in gradual changes to bedforms.

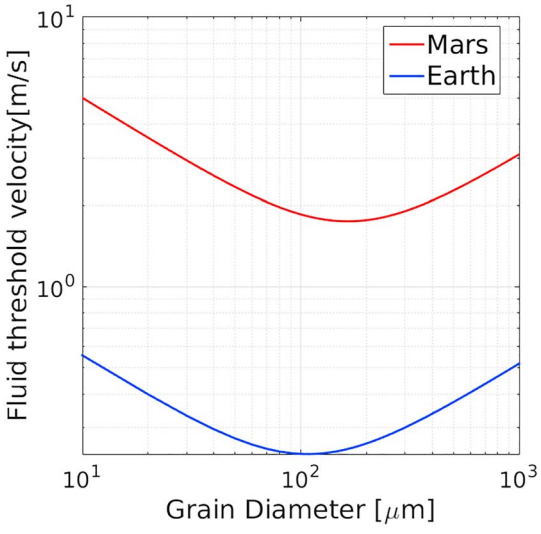


**Figure 2.** Fluid threshold velocity as a function of grain size for Earth (blue) and Mars (red) conditions. Both curves show a minimum around 100 $\mu$m. The calculations are based on Shao and Lu (2000) with $\gamma = 3 \cdot 10^{-4}$ interparticle force parameter. Note that the Martian fluid threshold velocity is much higher than that on Earth.

The goal of this paper is to evaluate the distribution of shear stress, $\tau$, and shear velocity, $u_*$, over simulated ripples produced by a

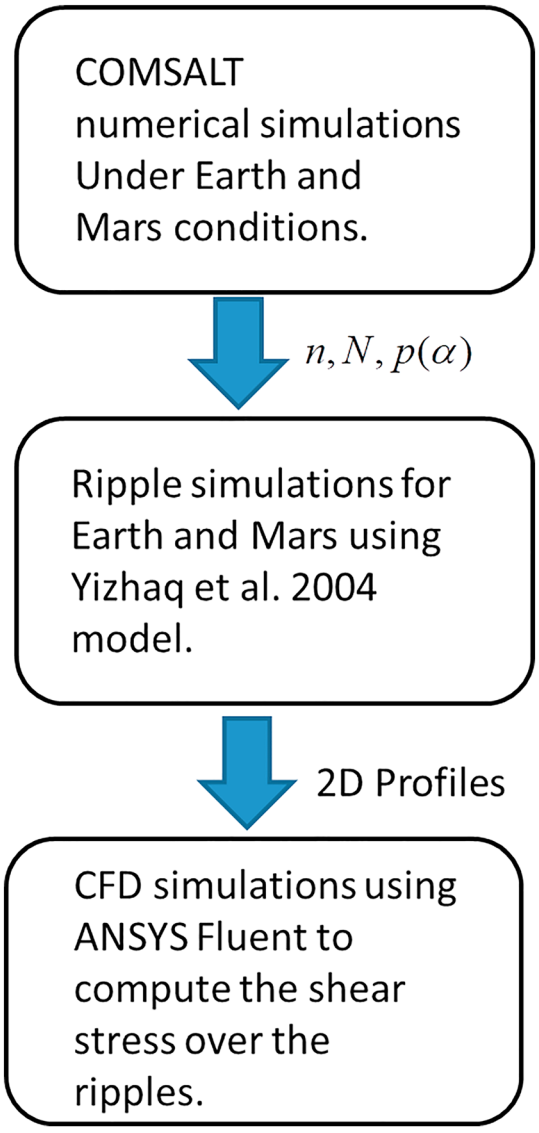


**Figure 3.** A schematic chart shows the procedure used for the calculation of the shear stress. The ripple model was run with parameters given by COMSALT under Earth and Martian conditions. The profiles produced by the ripple model were the input for ANSYS Fluent software to calculate the shear stress distribution over the ripples. CFD = computational fluid dynamics.

mathematical model under terrestrial and Martian conditions for two wind speeds (10 and 15 m/s). Figure 3 shows the procedure used for the calculation of the shear stress over the ripples. The distribution of the shear stress over ripple crests is important for predicting the entrainment from the crest. Despite this being one of several possible mechanisms for limiting ripple growth (Katra et al., 2014), its relative importance on Earth and Mars is not understood.

## 2. Materials and Methods

### 2.1. Ripple Model

To produce the ripple profiles for Earth and Mars, we used the COMSALT model for saltation (Kok & Renno, 2009) together with a spatiotemporal 2-D model for aeolian sand ripples (Yizhaq et al., 2004). This is the same method used in Yizhaq et al. (2014) to model small impact ripples at Eagle crater. COMSALT includes many of the features included in previous saltation models (e.g., Werner, 1990), and in addition it includes (1) a physically based parameterization of the splashing function (Kok & Renno, 2009), (2) a generalization of this splashing function to beds composed of polydisperse particles, and (3) a detailed consideration of the effect of turbulence in the boundary layer on particle trajectories, which agrees with wind tunnel experiments. Results of numerical simulations under Martian conditions indicate that saltation can be maintained on Mars by wind speeds an order of magnitude less than those required to initiate saltation mainly due to the low density Martian atmosphere (Kok, 2010b).

COMSALT simulations (Kok & Renno, 2009) were used to give the values of the parameters for saltation and reptation on Earth and Mars that were employed by the ripple model for simulating ripple profiles. Then these profiles were used by ANSYS Fluent, which is a computational fluid dynamics (CFD) commercial software (reference Cornell Fluent tutorials, n.d.; see section 2.2), to compute the shear stress distribution. Specifically, COMSALT supplies three parameters to the ripple model: the average number of reptating grains per impact of one saltating grain $n$, the number density of saltator impacts on a flat surface $N_{im}^{0}$, and the probability distribution of reptation lengths $p(\alpha)$.

The ripple model is based on the mathematical approach developed by Anderson (1987) and includes a modification to the reptation flux that depends on the local bed slope (Yizhaq et al., 2004). Within this framework, the role of saltating particles is to extract energy from the wind to maintain the reptation population. Thus, ripple formation is due entirely to spatial changes in the reptation flux. The 2-D model of sand transport is based on the Exner equation (Anderson, 1987; Yizhaq et al., 2004), which expresses the mass conservation:

$$(1-\lambda_p)\rho_p \frac{\partial h}{\partial t} = -\frac{\partial Q}{\partial x}, \tag{1}$$

where $h(x,t)$ is the local height of the bed at point $x$ and time $t$, $\lambda_p$ is the porosity of the bed (taken as 0.35), $\rho_p$ is the grain density, and $Q(x,t)$ is the sand flux, which includes both saltation ($Q_s$) and reptation ($Q_r$) fluxes. We further assume that saltation flux can be taken as uniform; thus, it does not contribute to ripple formation (i.e., $\partial Q_s/\partial x = 0$; for a different view of this assumption see Durán et al., 2014). Equation (1) thus provides the reptation flux, $Q_r$. The reptation flux at a certain point and time is expressed by the sum of all the reptating grains that pass through that point at that time. The grains have a probability distribution of

**Table 1**
*The Parameters Used in the Ripple Numerical Simulations, Which Were Calculated by the COMSALT Model*

| | $N^0_{im}$ [$m^{-2}/s$] | $n$ | $p(\alpha)$ |
|---|---|---|---|
| Earth | $1.32125 \cdot 10^8$ | 0.7288 | $a = 7.81{\cdot}10^{-5}$<br>$b = 0.170$<br>$c = 0.0235$<br>$s = 1.564$ |
| Mars | $1.75020 \cdot 10^6$ | 1.1748 | $a = 3.9{\cdot}10^{-4}$<br>$b = 0.215$<br>$c = 0.027$<br>$s = 1.241$ |

reptation lengths $p(\alpha)$, which mainly depend on the grain size and very weakly on the shear velocity (Yizhaq et al., 2014). The reptation flux is given by a double integral term that turns equation (1) into a complex integro-differential equation (Anderson, 1987):

$$Q_r = mn \int_0^{\infty} d\alpha p(\alpha) \int_{x-\alpha}^{x} N_{im}\left(x'\right) dx, \tag{2}$$

where $m$ is the mass of each particle. Because saltation flux is assumed to be spatially uniform and the impact angle, $\phi$, is constant (actually, it also has a narrow probability distribution that can be neglected in the context of this study; Schmerler et al., 2016), the number density of impacting grans, $N_{im}(x)$, varies only due to changes in the bed slope $h_x$. Based on geometrical considerations, we find (Yizhaq et al., 2004):

$$N_{im}(x) = N^0_{im} \frac{1 + h_x \cot\phi}{\sqrt{1 + h_x^2}}. \tag{3}$$

Equation (3) breaks down when the lee slope of the ripple exceeds the impact angle $\phi$ of the impinging saltating particles (i.e., when $1 + h_x \cot\phi < 0$) since the ratio $N_{im}/N^0_{im}$ becomes negative, which is unphysical. In these cases, we added the constraint that the impact flux is zero. We also applied this condition for the shadow zone where the impact rate is zero by definition. Thus, we used a complete shadowing effect (Manukyan & Prigozhin, 2009) below the line defined by the saltation path of a grain that touches the crest. Equation (2) was modified to include a correction of the reptation flux that is smaller at the stoss slope and larger at the lee slope of the ripple (Yizhaq et al., 2004). The physical explanation for this modification is that part of the kinetic energy of the impacting saltator is imparted to surface grains, which vibrate rapidly, and as a result can creep down the slope. This flow of particles is known as "impact-induced gravity flow" (Hardisty & Whitehouse, 1988). This mechanism acts to reduce the flux on the windward slope and to increase it on the lee face due to addition of rolling grains (see also Prigozhin, 1999). The full model that includes the reptation flux modification is given by

$$h_t = -Q_0 \partial_x [(1-\mu) Q_r], \tag{4}$$

where the parameter $\mu$ heuristically includes the correction to reptation flux discussed above, and $Q_0 = mnN^0_{im} \cot\phi/\rho_b(1-\lambda_p)$. The basic parameters ($N^0_{im}$, $n, p(\alpha)$) used in the model are given by COMSALT, which simulates Martian and Earth environments for $u_* = 0.5$ m/s and for 100-μm sand particles (see Yizhaq et al., 2014). The computed probability distribution of reptation lengths is given by

$$p(\alpha) = s\left(1 - \exp\left(-\sqrt{x/a}\right)\right)(b/x)\exp\left(-\sqrt{x/c}\right), \tag{5}$$

where $s$, $a$, $b$, and $c$ are numerical constants (see Table 1) and $\int_0^{\infty} p(\alpha) d\alpha = 1$.

Equation (4) was solved numerically by using an explicit second-order finite difference scheme with periodic boundary and random initial conditions. The integral terms were calculated by using the composite trapezoid rule, and the time integration was carried out by using the second-order Adams-Bashforth rule (Fausett, 1999). The grid consisted of 2,048 points for a spatial dimension of 2 m (i.e., $\Delta x \approx 1$ mm) and a time step of 0.005 s. Wind velocity and direction (from left to right) are constant during the simulations. Although ripples on Earth can be formed within minutes (e.g., Anderson, 1990; Andreotti et al., 2006; Rasmussen et al., 2015; Schmerler et al., 2016), the lower Martian air density results in a much lower saltator impact rate (~2 order of magnitudes) on Mars (~$10^6$ $m^{-2}/s$ for $u_* = 0.5$ m/s) than on Earth (~$10^8$ for $u_* = 0.5$ m/s), making Martian ripple formation a much slower process than on Earth. As the model does not have a feedback between ripple topography and wind flow that can account for a final steady state, the modeled ripples can continue to grow, although with a decreasing rate, because the difference in their height decreases in time resulting in slowing the rate of merging events between adjacent ripples (see Figure 7 in Yizhaq et al., 2004). In the current study, we chose larger modeled Martian ripples than terrestrial ripples to show that

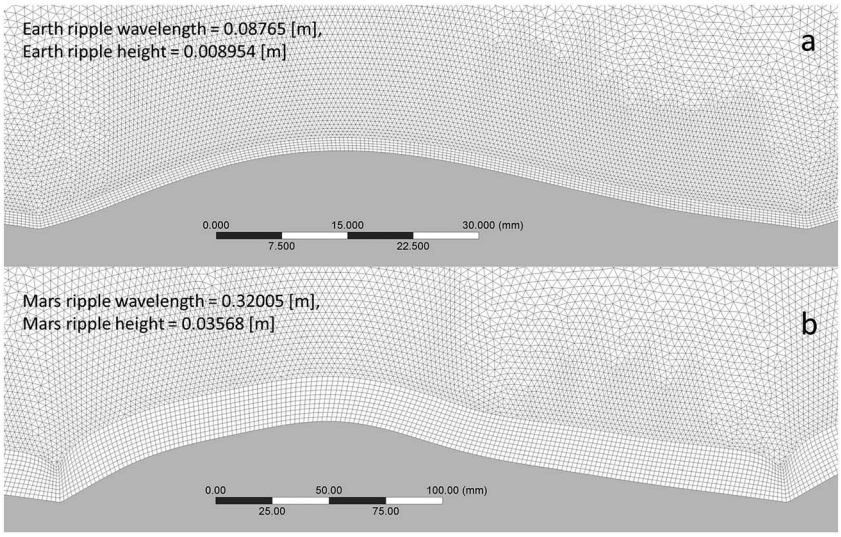


**Figure 4.** The two profiles used in the ANSYS Fluent simulation for (a) Earth and (b) Mars. The profiles were produced by numerical simulations of the ripple model (equation (1)). Note that the Martian ripple is larger (in both height and wavelength) than the terrestrial ripple.

the shear velocity over the Martian ripples is below the fluid threshold whereas for the smaller terrestrial ripples the shear velocity is above the fluid threshold. We leave the study of even larger Martian ripples, which requires a huge numerical effort (larger grid and a much longer time) to simulate, for a future study.

### 2.2. CFD Method

ANSYS Fluent (ANSYS Manual) was used to study the distribution of shear stress over the ripples. The details of the numerical technique are given below.

#### 2.2.1. Geometry of the Control Grid

A two-dimensional rectangular control grid with a height of 1 m and a length of 12 m was used in the simulations. The control grid is divided into two sections in the flow direction: a section with ripples along 7 m and a smooth plate downwind having a length of 5 m (see Figure S1 in the supporting information). This geometry was chosen as a compromise between numerical efficiency and high enough spatial resolution. It is short enough to be numerically efficient with reasonably fine mesh while long enough to ensure that the mean flow and the small-scale flow features near the ripples do not change considerably downwind that is to decrease the influence of the boundary conditions on the flow. The upper boundary of the control volume is a fixed smooth wall. The ripple profiles are asymmetric (Figure 4), and their shapes were obtained by the numerical simulations of the ripple model described above (for $u_* = 0.5$ m/s). We used an adaptive mesh that is finer near the undulating bed to capture fine details of the flow. The mesh consists of quadrilateral and triangular plane elements (Figure 4).

#### 2.2.2. Setup and Solution

To find a numerical solution, we used a steady state density-based two-dimensional solver. The parameters for Earth and Mars atmospheres are presented in Table 2 (Kok et al., 2012). At the upper and lower boundaries of the grid we used no-slip solid wall boundary conditions for velocity, and constant temperature pertinent to Earth and Mars atmospheres at the walls. At the inlet we used a uniform normal-to-plane flow with turbulent intensity of 5%, which is a moderate value (turbulence intensities greater than 10% are considered high, according to the ANSYS Manual) and turbulent viscosity ratio of 10 (typical for most external flows where boundary layers developed freely). We applied the SST (shear stress transport) k-omega turbulence model (CFD-Wiki, 2011; Menter, 1994) since the main goal of this work was to find the shear stress distribution at the surface.

As in all turbulence models, the SST model has a number of free parameters that must be defined before running the simulation. We used the default values of the free parameters given by ANSYS

**Table 2**
*The Parameters for Earth and Mars Atmospheres Used in the ANSYS Fluent Simulations*

| Parameter's description | Temperature | Acceleration due to gravity | Surface atmospheric pressure | Surface atmospheric density | Specific heat | Thermal conductivity | Kinematic viscosity | Viscosity | Molar mass |
|---|---|---|---|---|---|---|---|---|---|
| Parameter's Symbol and units | $T\,[k]$ | $g\,\left[\frac{m}{s^2}\right]$ | $P\,[Pa]$ | $\rho\,\left[\frac{kg}{m^3}\right]$ | $C_p\,\left[\frac{J}{Kg \cdot K}\right]$ | $k\,\left[\frac{W}{m \cdot K}\right]$ | $\nu\,\left[\frac{m^2}{s}\right]$ | $\mu\,\left[\frac{kg}{m \cdot s}\right]$ | $m_w\,\left[\frac{kg}{Kmol}\right]$ |
| *Earth* | 293 | 9.81 | 101,325 | 1.205 | 1,005 | 0.0257 | $15.11 \cdot 10^{-6}$ | $1.8208 \cdot 10^{-5}$ | 28.966 |
| *Mars* | 213 | 3.711 | 600 | 0.014684 | 743.246 | 0.0257 | $6 \cdot 10^{-4}$ | $1.2 \cdot 10^{-5}$ | 43.34 |

Fluent (see section 2.2.3). To assure full convergence for the solver, we used the solution steering option, which is a solver convergence tool in ANSYS Fluent for density-based steady state solutions. The blending parameter in the steering option specifies the ratio of the second-order blending accuracy to the first-order accuracy. The default value is 100%, but typical values are 75% or 50%, which demand less computations. This option is applicable only when higher-order discretization scheme is used. A blending parameter of 75% was used, and default values were used for the other parameters of the steering option. In the computations we used the equation of an ideal gas as the equation of state for the atmospheres of Earth and Mars. The density-based solver solves Reynolds-averaged Navier-Stokes equations. These equations include three partial differential equations: modified conservation equations (mass, momentum, and energy) coupled with two ordinary differential equations for turbulent kinetic energy and turbulent dissipation. The solution of these equations is an ensemble-averaged velocity field with spatial distributions of turbulent kinetic energy and turbulent dissipation. Note that we considered a single phase flow over a rough surface without taking into account the effect of the saltation cloud on the flow.

### 2.2.3. Code Validation

Numerical results were compared with the known analytical solutions for laminar and turbulent flow over a flat plate under Earth ambient pressure (see Figure S2). Mesh verification was done by increasing mesh density to ensure that the chosen mesh was fine enough to capture the details of the flow. Especially, we verified that the mesh is dense enough to resolve the fine structure of the flow close

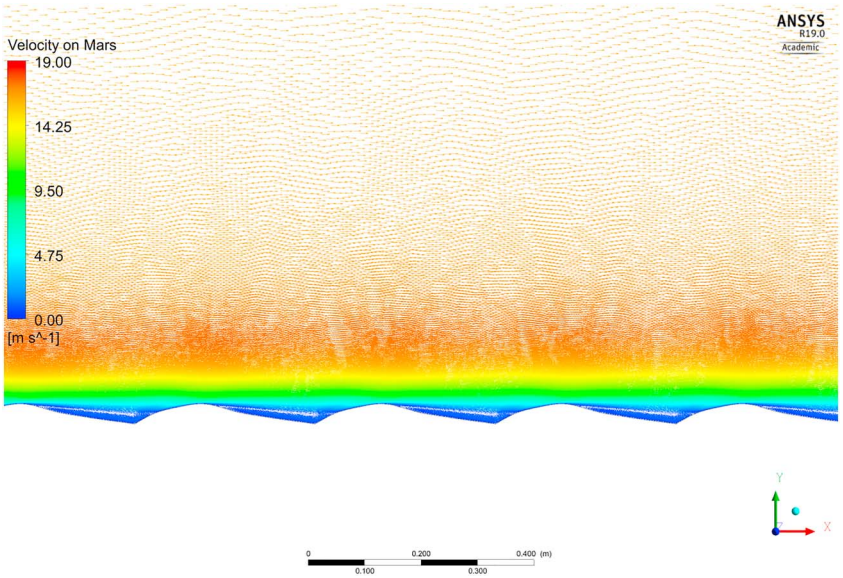


**Figure 5.** Wind velocity distribution over simulated ripples under Mars conditions for inlet velocities of 15 m/s. Note that the wind velocity is larger at the ripple crests. Vortices form between successive ripples, as shown more clearly in Figures 8b and 9b.

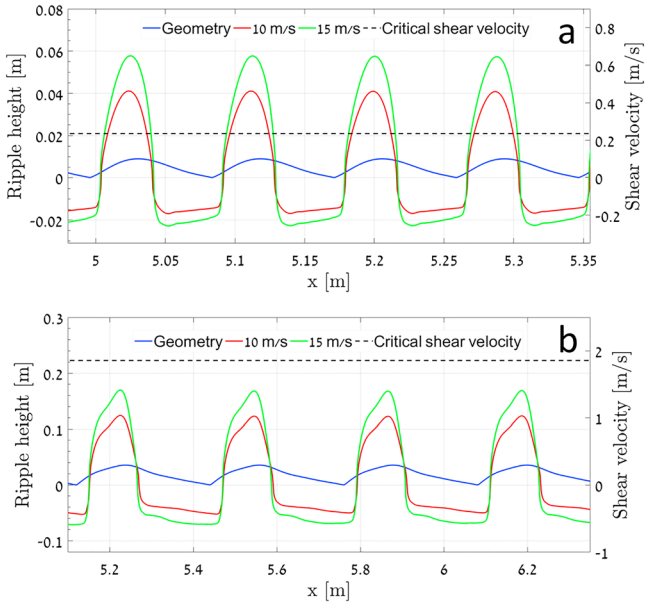


**Figure 6.** Shear velocity over the ripples for two inlet wind velocities 10 m/s (red) and 15 m/s (green) for (a) Earth and (b) Mars. Ripple height is shown in blue. The flow for Mars conditions is slightly asymmetric because of the shape of the windward slope. The dashed line shows the calculated fluid shear velocity threshold velocity based on Shao and Lu (2000) for 100 μm particles (1.86 m/s for Mars and 0.247 m/s for Earth). For Earth conditions the shear velocity is above the fluid threshold velocity (i.e., $u_* > u_{*t}$) at the crest and over part of the windward (stoss) slope, whereas under Mars conditions $u_* < u_{*t}$ for the entire ripple profile.

to the ripples (such as the vortices between successive ripples) in the region with the wall coordinate $y^+ = yu_*/\nu < 14$ (for more details see Landau and Lifshitz, p. 175, Figure 31) where $\nu$ is the fluid's kinematic viscosity of air defined as $\nu = \mu/\rho$ (see Table 2).

## 3. Results

We used two inlet wind velocities of 10 and 15 m/s to compute the shear stress distribution over the modeled ripples. As a wind speed of 15 m/s was already strong enough to show a clear difference in the shear stress distributions over the ripples between Earth and Mars, and as the highest wind speed measured at the Phoenix landing site was 16 m/s (Holstein-Rathlou et al., 2010), we did not perform any simulations with stronger winds. These two wind velocities were sufficient to support our main hypothesis that the shear velocity over Martian ripples is below the fluid threshold, whereas under Earth conditions it is above the fluid threshold thus limiting their growth.

The wind velocity distribution over the ripples for Mars conditions at 15 m/s is shown in Figure 5 (for Mars at 10 m/s and for Earth conditions at both inlet velocities, see Figures S3–S5).

Shear stress and shear velocity distribution over the ripples for Earth and Mars for inlet wind velocities of 10 and 15 m/s are shown in Figures 6 and 7, respectively.

Interestingly, the simulated flow shows the existence of vortices between the adjoining ripples (Figures 8 and 9 and Bar et al., 2016). Clearly, the development of the vortices depends on the morphometry of the ripples and the incoming flow velocity and fluid characteristics. These small vortices are similar to the lee eddies observed in simulated flow over a barchan dune (Herrmann et al., 2005). Evidence for the presence of such vortices between successive ripples was found in wind tunnel experiments of flow over ripples by Tong and Huang (2012).

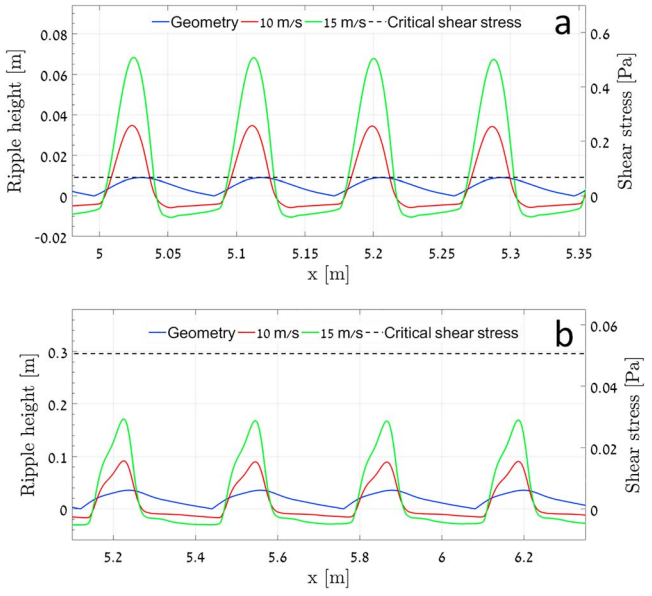


**Figure 7.** As in Figure 6 but now showing the same results in terms of shear stress: (a) Earth and (b) Mars.

## 4. Discussion

In this study ANSYS Fluent CFD simulations with ripple profiles demonstrate that shear stress along Martian ripple crests is below the fluid threshold shear stress for motion to occur via direct fluid drag. In contrast, the CFD simulations over smaller terrestrial ripple profiles show that the shear velocity at the crests is above the fluid threshold. This is consistent with their smaller size, as erosion of particles at the crest limits ripple growth. It is important to note that our analysis does not account for the effect of a saltation cloud, which will decrease the shear stress at the surface (Kok et al., 2012; Tong & Huang, 2012). Our results thus overestimate the shear stress during saltation. This effect is much more significant for Earth than for Mars where the sand flux is generally an order of magnitude smaller (see Table 1; Chojnacki et al., 2017). In addition, the saltation flux on Mars will further reduce the simulated shear velocity over the ripples; thus, our results suggest that for ambient wind speeds up to at least 15 m/s, no direct entrainment would occur from the ripple crests.

Since our simulation does not include the effect of saltating particles on the flow, the shear stress distribution over sand ripples is more important at the initial stage of saltation where sand transport

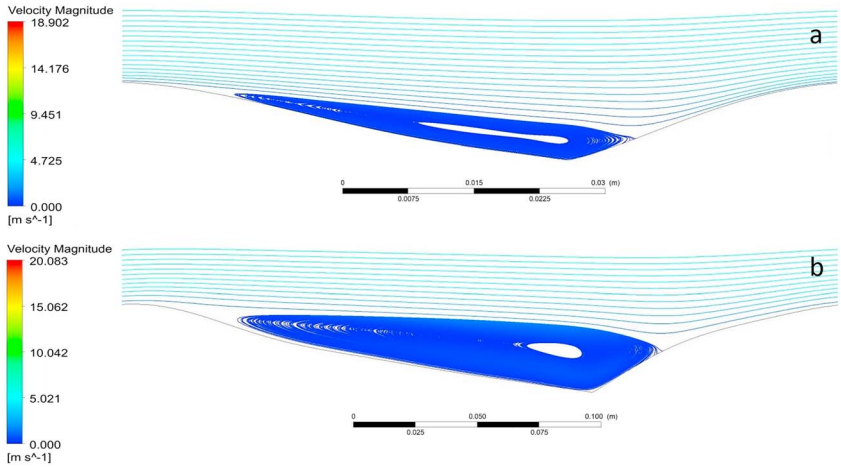


**Figure 8.** Close-up of the vortices that formed between successive ripples for (a) Earth and (b) Mars for 15 m/s wind speed.

occurs due to direct wind entrainment. Over this short time frame, sand grains from the crests will be dislodged as the shear stress at the surface exceeds the fluid threshold, thus decreasing ripple height.

Although our simulated ripples are quite small compared to the large ripples observed on Mars (e.g., Lapotre et al., 2016), the smaller shear stress at the crest may explain why impact ripples can be larger on Mars. Specifically, the ripples on Mars can still grow due to saltation that occurs at low wind speeds above the impact threshold (Sullivan & Kok, 2017). Thus, the large ripples on Mars can form under the same impact mechanism acting for small ripples without the need for the wind-drag formation hypothesis (Lapotre et al., 2018a, 2018b). However, further work is needed to explore our hypothesis that the same impact mechanism can produce the multiple scales of ripples on Mars.

This work should include (i) the effect of the saltation cloud on the flow and (ii) CFD simulations of shear stress over large ripples like the ones found by Curiosity at Gale Crater (Lapotre et al., 2016) and for more common sand grain sizes observed on Mars (e.g., 200 and 300 μm).

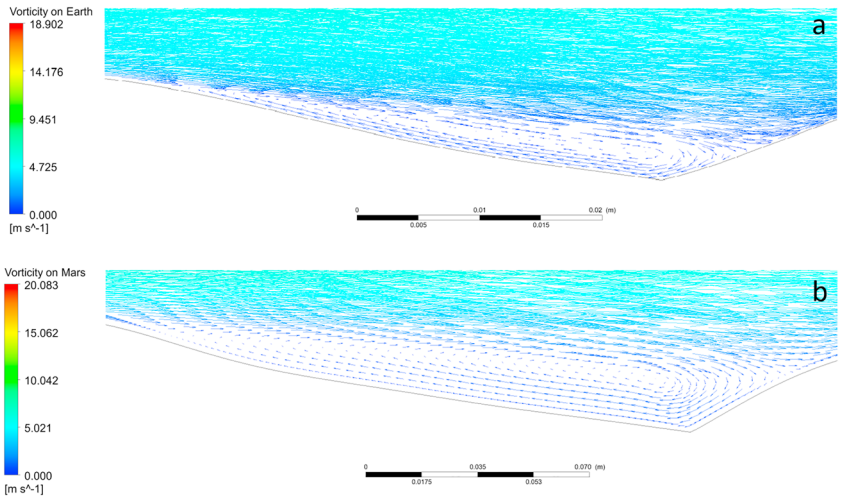


**Figure 9.** Streamlines of the flow inside the trough between two successive ripples for (a) Earth and (b) Mars for 15 m/s wind speed from left to right.

## 5. Conclusions

The existence of very large ripples on Mars lacking exact terrestrial analogues is not fully understood at this time and is still a matter of conjecture and debate (Lapotre et al., 2018a, 2018b; Sullivan et al., 2018; Vaz et al., 2017). In this study, ANSYS Fluent CFD simulations over simulated sand ripples illustrate the differences in shear stress expected at ripple crests on Earth and Mars under two test inlet wind speeds. The Martian ripple profile was three times larger in the experiments than the terrestrial ripple profile but still several factors smaller than the largest ripples encountered by Mars rovers. Despite this, shear velocities along Martian ripple crests did not reach fluid threshold, while at the crests of the smaller terrestrial ripples, fluid threshold was exceeded at the same test inlet wind speeds. These results indicate that ripples can grow larger on Mars than on Earth, because for typical Martian wind speeds the shear velocity at the ripple crests is below the fluid threshold. The results of this study are useful for understanding aeolian process involved in ripple formation under Martian atmospheric conditions. Further studies are needed to verify this conclusion for more realistic larger Martian ripples and for higher shear velocities.

**Acknowledgments**
This work was supported by the German-Israeli Foundation for Scientific Research and Development (GIF Research Grant 1143-60.8/2011), by the Israel Science Foundation governed by the Israeli Academy of Sciences (Grant 1210/15) and by NASA's Outer Planets Research Program (Grant 131186). The authors would like to thank to the Associate Editor Claire Newman, Jim Zimbelman, and Timothy N. Titus for their valuable comments and suggestions. There is no real or perceived financial conflicts of interests for any author. There are no affiliations for any author that may be perceived as having a conflict of interest with respect to the results of this paper. Data supporting the conclusions can be found in Yizhaq et al. (2004) and Yizhaq et al. (2014) and in Tables 1 and 2 and in the supporting information.

## References

Allen, J. R. L. (1968). *Current ripples: Their relation to patterns of water and sediment motion*. Amsterdam: North-Holland Pub. Co.

Anderson, R. S. (1987). A theoretical model for aeolian impact ripples. *Sedimentology*, *34*(5), 943–956. https://doi.org/10.1111/j.1365-3091.1987.tb00814.x

Anderson, R. S. (1990). Eolian ripples as examples of self-organization in geomorphological systems. *Earth-Science Reviews*, *29*(1-4), 77–96. https://doi.org/10.1016/0012-8252(0)90029-U

Anderson, R. S., & Bunas, K. L. (1993). Grain size segregation and stratigraphy in aeolian ripples modeled with a cellular automaton. *Nature*, *365*(6448), 740–743. https://doi.org/10.1038/365740a0

Andreotti, B., Claudin, P., & Pouliquen, O. (2006). Aeolian sand ripples: Experimental study of fully developed states. *Physical Review Letters*, *96*(2), 028001. https://doi.org/10.1103/PhysRevLett.96.028001

Bagnold, R. A. (1941). *The physics of blown sand and desert dunes*. London: Methuen.

Baker, M. M., Newman, C. E., Lapotre, M. G. A., Sullivan, R., Bridges, N. T., & Lewis, K. W. (2018). Coarse sediment transport in the modern Martian environment. *Journal of Geophysical Research: Planets*, *123*, 1380–1394. https://doi.org/10.1002/2017JE005513

Bar, N., Elperin, T., Katra, I., & Yizhaq, H. (2016). Numerical study of shear stress distribution at sand ripple surface in wind tunnel flow. *Aeolian Research*, *21*, 125–130. https://doi.org/10.1016/j.aeolia.2016.04.007

Basu, S., Richardson, M. I., & Wilson, R. J. (2004). Simulation of the Martian dust cycle with GFDL Mars GCM. *Journal of Geophysical Research*, *109*, E11006. https://doi.org/10.1029/2004JE002243

Bridges, N. T., Ayoub, F., Leprince, S., Lucas, A., & Mattson, S. (2012). Earth-like sand fluxes on Mars. *Nature*, *485*(7398), 339–342. https://doi.org/10.1038/nature11022

Bridges, N. T., Geissler, P. E., McEwen, A. S., Thomson, B. J., Chuang, F. C., Herkenhoff, K. E., et al. (2007). Windy Mars: A dynamic planet as seen by the HiRISE camera. *Geophysical Research Letters*, *34*, L23205. https://doi.org/10.1029/2007GL031445

CFD-Wiki (2011). SST k-omega model. https://www.cfd-online.com/Wiki/SST_k-omega_model, www.cfd-online.com

Chojnacki, M., Burrm, D. M., Moersch, J. F., & Michaeles, T. I. (2011). Orbital observations of contemporary dune activity in Endeavor Crater, Meridiani Planum, Mars. *Journal of Geophysical Research*, *116*, E00F19. https://doi.org/10.1029/2010JE003675

Chojnacki, M., Urso, A., Fenton, L. K., & Michaeles, T. I. (2017). Aeolian dune sediment flux heterogeneity in Meridiani Planum, Mars. *Aeolian Research*, *26*, 73–88. https://doi.org/10.1016/j.aeolia.2016.07.004

Claudin, P., & Andreotti, B. (2006). A scaling law for aeolian dunes on Mars, Venus, Earth, and for subaqueous ripples. *Earth and Planetary Science Letters*, *252*(1-2), 30–44. https://doi.org/10.1016/j.epsl.2006.09.004

Cornell Fluent tutorials (n.d.). https://confluence.cornell.edu/display/simulation/fluent+learning+modules

Durán, O., Claudin, P., & Andreotti, B. (2014). Direct numerical simulations of aeolian sand ripples. *PNAS*, *111*(44), 15,665–15,668. https://doi.org/10.1073/pnas.1413058111

Ewing, R. C., Lapotre, M. G. A., Lewis, K. W., Day, M., Stein, N., Rubin, D. M., et al. (2017). Sedimentary processes of the Bagnold Dunes: Implications for the eolian rock record of Mars. *Journal of Geophysical Research: Planets*, *122*, 2544–2573. https://doi.org/10.1002/2017JE005324

Fausett, L. V. (1999). *Applied numerical analysis using Matlab*, (07458). Upper Saddle River, NJ: Prentice Hall.

Greeley, R., Leach, R., White, B., Iversen, J., & Pollack, J. (1980). Threshold windspeeds for sand on Mars: Wind tunnel simulations. *Geophysical Research Letters*, *7*(2), 121–124. https://doi.org/10.1029/GL007i002p00121

Hardisty, R. J. S., & Whitehouse, J. (1988). Evidence for a new sand transport process from experiments on Saharan dunes. *Nature*, *332*(6164), 532–534. https://doi.org/10.1038/332532a0

Herrmann, H. J., Andrade, J. S., Schatz, V., Sauermann, G., & Parteli, E. J. R. (2005). Calculation of the separation streamlines of barchans and transverse dunes. *Physica A*, *357*(1), 44–49. https://doi.org/10.1016/j.physa.2005.05.057

Holstein-Rathlou, C., Gunnlaugsson, H. P., Merrison, J. P., Bean, K. M., Cantor, B. A., Davis, J. A., et al. (2010). Winds at the Phoenix landing site. *Journal of Geophysical Research*, *115*, E00E18. https://doi.org/10.1029/2009JE003411

Iversen, J. D., & White, B. R. (1982). Saltation thresholds on Earth, Mars, and Venus. *Sedimentology*, *29*(1), 111–119. https://doi.org/10.1111/j.1365-3091.1982.tb01713.x

Katra, I., Yizhaq, H., & Kok, J. F. (2014). Mechanisms limiting the growth of aeolian megaripples. *Geophysical Research Letters*, *41*, 858–865. https://doi.org/10.1002/2013GL058665

Kok, J. F. (2010a). An improved parameterization of wind-blown sand flux on Mars that includes the effect of hysteresis. *Geophysical Research Letters*, *37*, L12202. https://doi.org/10.1029/2010GL043646

Kok, J. F. (2010b). Differences in the wind speeds required for initiation versus continuation of sand transport on Mars: Implications for dunes and sand storms. *Physical Review Letters*, *104*(7), 074502. https://doi.org/10.1103/PhysRevLett.104.074502

Kok, J. F., Parteli, E. J. R., Michaels, T., & Bou Karam, D. (2012). The physics of wind-blown sand and dust. *Reports on Progress in Physics*, *75*(10), 106901. https://doi.org/10.1088/0034-4885/75/10/106901

Kok, J. F., & Renno, N. O. (2009). A comprehensive numerical model of steady state saltation (COMSALT). *Journal of Geophysical Research*, *114*, D17204. https://doi.org/10.1029/2009 JDO11702

Lämmel, M., Meiwald, A., Yizhaq, H., Tsoar, H., Katra, I., & Kroy, K. (2018). Aeolian sand sorting and megaripple formation. *Nature Physics*, *14*(7), 759–765. https://doi.org/10.1038/s41567-018-0106-z

Lapotre, M. G. A., Ewing, R. C., Lamb, M. P., Fischer, W. W., Grotzinger, J. P., Rubin, D. M., et al. (2016). Large wind ripples on Mars: A record of atmospheric evolution. *Science*, *353*(6294), 55–58. https://doi.org/10.1126/science.aaf3206

Lapotre, M. G. A., Ewing, R. C., Weitz, C. M., Lewis, K. W., Lamb, M. P., Ehlmann, B. L. & Bridges, N. T. (2018a). Morphologic diversity of Martian ripples: implications for low-intensity transport as a mechanism for large-ripple formation, in X International Conference on Aeolian Research

Lapotre, M. G. A., Ewing, R. C., Weitz, C. M., Lewis, K. W., Lamb, M. P., Ehlmann, B. L., & Rubin, D. M. (2018b). Morphologic diversity of Martian ripples: Implications for large-ripple formation. *Geophysical Research Letters*, *45*, 10,229–10,239. https://doi.org/10.1029/2018GL079029, https://doi.org/10.1029/2018GL079029

Malin, M. C., & Edgett, K. S. (2001). Mars Global Surveyor Mars Orbiter Camera: Interplanetary cruise through primary mission. *Journal of Geophysical Research*, *106*(E10), 23429–23570. https://doi.org/10.1029/2000JE001455

Manukyan, E., & Prigozhin, L. (2009). Formation of aeolian ripples and sand sorting. *Physical Review E*, *79*(3), 031303. https://doi.org/10.1103/PhysRevE.79.031303.

Menter, F. R. (1994). Two-equation eddy-viscosity turbulence models for engineering applications. *AIAA Journal*, *32*(8), 1598–1605. https://doi.org/10.2514/3.12149

Prigozhin, L. (1999). Nonlinear dynamics of aeolian sand ripples. *Physical Review E*, *60*(1), 729–733. https://doi.org/10.1103/PhysRevE.60.729

Rasmussen, K. R., Valance, A., & Merrison, J. (2015). Laboratory studies of aeolian sediment transport processes on planetary surfaces. *Geomorphology*, *244*, 74–94. https://doi.org/10.1016/j.geomorph.2015.03.041

Schmerler, E., Katra, I., Kok, J. F., Tsoar, H., & Yizhaq, H. (2016). Experimental and numerical study of Sharp's shadow zone hypothesis on sand ripple wavelength. *Aeolian Research*, *22*, 37–46. https://doi.org/10.1016/j.aeolia.2016.05.006

Schofield, J. T., Barnes, J. R., Crisp, D., Haberle, R. M., Larsen, S., Magalhães, J. A., et al. (1997). The Mars Pathfinder atmospheric structure investigation meteorology (ASI/MET) experiment. *Science*, *278*(5344), 1752–1758. https://doi.org/10.1126/science.278.5344.1752

Seppälä, M., & Lindé, K. (1978). Wind tunnel studies of ripple formation. *Geografiska Annaler. Series A, Physical Geography*, *60*(1–2), 29–42. https://doi.org/10.1080/04353676.1978.11879961

Shao, Y., & Lu, H. (2000). A simple expression for wind erosion threshold friction velocity. *Journal of Geophysical Research*, *105*(D17), 22,437–22,443. https://doi.org/10.1029/2000JD900304

Sharp, R. P. (1963). Wind ripples. *Journal of Geology*, *71*(5), 617–636. https://doi.org/10.1086/626936

Silvestro, S., Fenton, L. K., Vaz, D. A., Bridges, N. T., & Ori, G. G. (2010). Ripple migration and dune activity on Mars: Evidence for dynamic wind processes. *Geophysical Research Letters*, *37*, L20203. https://doi.org/10.1029/2010GL044743

Silvestro, S., Vaz, D. A., Fenton, L. K., & Geissler, P. E. (2011). Active aeolian processes on Mars: A regional study in Arabia and Meridiani Terrae. *Geophysical Research Letters*, *38*, L20201. https://doi.org/10.1029/2011GL048955

Silvestro, S., Vaz, D. A., Yizhaq, H., & Esposito, F. (2016). Dune-like dynamic of Martian Aeolian large ripples. *Geophysical Research Letters*, *43*, 8384–8389. https://doi.org/10.1002/2016GL070014

Sullivan, R., Arvidson, R., Bell, J. F. III, Gellert, R., Golombek, M., Greeley, R., et al. (2008). Wind-driven particle mobility on Mars: Insights from Mars Exploration Rover observations at "El Dorado" and surroundings at Gusev crater. *Geophysical Research Letters*, *113*, E06S07. https://doi.org/10.1029/2007JE003101

Sullivan, R., Banfield, D., Bell, J. F. III, Calvin, W., Fike, D., Golombek, M., et al. (2005). Aeolian processes at the Mars Exploration Rover Meridiani Planum landing site. *Nature*, *436*(7047), 58–61. https://doi.org/10.1038/nature03641

Sullivan, R., & Kok, J. F. (2017). Aeolian saltation on Mars at low wind speeds. *Geophysical Research Letters*, *122*, 2111–2143. https://doi.org/10.1002/2017JE005275

Sullivan, R.J., Kok, J. F., Yizhaq, H., Siminovich, A., Elperin, T. & Katra, I. (2018). Low dynamic wind pressures on Mars allow a broad continuum of aeolian ripple sizes, in X International Conference on Aeolian Research.

Tong, D., & Huang, N. (2012). Numerical simulation of saltating particles in atmospheric boundary layer over flat bed and sand ripples. *Journal of Geophysical Research*, *117*, D16205. https://doi.org/10.1029/2011JD017424

Vaz, D. A., Silvestro, S., Sarmento, P. T. K., & Cardinale, M. (2017). Migrating meter-scale bedforms on Martian dark dunes: Are terrestrial aeolian ripples good analogues? *Aeolian Research*, *26*, 101–116. https://doi.org/10.1016/j.aeolia.2016.08.003

Werner, B. T. (1990). A steady-state model of wind-blown sand transport. *Journal of Geology*, *98*(1), 1–17. https://doi.org/10.1086/629371

Wilson, I. G. (1972). Aeolian bedforms-their development and origins. *Sedimentology*, *19*(3-4), 173–210. https://doi.org/10.1111/j.1365-3091.1972.tb00020.x

Yizhaq, H., Balmforth, N. J., & Provenzale, A. (2004). Blown by wind: Nonlinear dynamics of aeolian sand ripples. *Physica D*, *195*(3-4), 207–228. https://doi.org/10.1016/j.physd.2004.03.015

Yizhaq, H., Katra, I., Isenberg, O., & Tsoar, H. (2012). Evolution of megaripples from a flat bed. *Aeolian Research*, *6*, 1–12. https://doi.org/10.1016/j.aeolia.2012.05.001

Yizhaq, H., Kok, J. F., & Katra, I. (2014). Basaltic sand ripples at Eagle crater as indirect evidence for the hysteresis effect in Martian saltation. *Icarus*, *230*, 143–150. https://doi.org/10.1016/j.icarus.2013.08.006

Zimbelman, J. R. (2000). Non-active dunes in the Acheron Fossae region of Mars between the Viking and Mars Global Surveyor eras. *Geophysical Research Letters*, *27*(7), 1069–1072. https://doi.org/10.1029/1999GL008399